Construction and Building Materials 239 (2020) 117883

Contents lists available at ScienceDirect

Construction and Building Materials

journal homepage: www.elsevier.com/locate/conbuildmat

Influence of accelerator type and dosage on the durability of wet-mixed sprayed concrete against external sulfate attack

Renan P. Salvador [a,b,*], Dimas A.S. Rambo [b], Roberto M. Bueno [b], Silvio R. Lima [b], Antonio D. Figueiredo [a]

[a] Department of Civil Construction Engineering, Polytechnic School of University of São Paulo, Professor Almeida Prado Av, Trav 2, 83, 05424-970 São Paulo, Brazil
[b] Department of Civil Engineering, São Judas Tadeu University, 546 Taquari St., 03166-000 São Paulo, Brazil

HIGHLIGHTS

- Accelerators reduce the durability of sprayed concrete against ESA.
- Ettringite formation is directly related to the final SO_3/Al_2O_3 ratio of the matrix.
- Deterioration is more pronounced when alkaline accelerators are employed.
- The lower the SO_3/Al_2O_3 ratio, the lower the concrete strength after ESA.

ARTICLE INFO

Article history:
Received 15 July 2019
Received in revised form 13 December 2019
Accepted 15 December 2019
Available online 23 December 2019

Keywords:
Sprayed concrete
Accelerator
External sulfate attack
Mechanical strength
Durability

ABSTRACT

External sulfate attack in concrete comprises a series of interdependent processes resulting from the interaction of sulfate ions from the external environment and cement phases, resulting in matrix degradation. To obtain a sulfate-resisting matrix, C_3A content in cement and water/cement ratio must be controlled. In sprayed concrete, accelerator type and dosage and the interaction between cement and accelerator are important parameters that control sprayed concrete strength and may influence the durability of the matrix. In this context, the objective of this study is to evaluate how accelerator type and dosage influence the durability of sprayed concrete exposed to a sulfate solution. Samples were analyzed by XRD, TGA, SEM, length change, US propagation velocity, compressive strength and water accessible porosity for 270 days. Results showed that sprayed concrete produced with accelerators presents a high deterioration rate due to sulfate attack. Kinetics of specimen expansion and reduction of compressive strength are directly related to the final SO_3/Al_2O_3 ratio of the matrix. This study may be useful to understand how external sulfate attack occurs in sprayed concrete and to develop prediction models and guidelines.

1. Introduction

External sulfate attack (ESA) is a complex phenomenon that plays an important role in assessing the long-term durability of cement-based materials exposed to a sulfate-rich environment [1–3]. It is an interdependent process, comprising dissolution of phases, ionic diffusion and precipitation reactions [4–6]. The main deleterious phase formed by ESA is ettringite, although gypsum may me formed when solutions containing a high sulfate concentration are employed [4,7,8]. Thaumasite may also be formed in concretes subjected to temperatures of 5 °C, approximately [9,10]. The formation of these phases generates expansion, cracking and loss of strength [11,12].

A potential risk of ESA in a concrete structure involves a humid external environment rich in sulfate ions and a permeable concrete matrix [6,13]. In order to minimize the risks of sulfate attack and its detrimental effects, building and structural codes specify precautionary measures to design sulfate-resisting cementitious matrices [14–16]. In order to reduce the probability of sulfate attack, the C_3A content in cement must be reduced in order to have a low amount of aluminate hydrates in the matrix [17], the water/cement ratio must be reduced to decrease the permeability of the matrix [1], and the matrix strength must be increased in order to reduce crack formation due to the forces caused by ettringite formation [18].

Sprayed concrete may present a high vulnerability to ESA because it remains in direct contact with the substrate and is

* Corresponding author at: Department of Civil Engineering, São Judas Tadeu University, 546 Taquari St., 03166-000 São Paulo, Brazil.
E-mail address: prof.renansalvador@usjt.br (R.P. Salvador).

https://doi.org/10.1016/j.conbuildmat.2019.117883
0950-0618/

exposed to the external environment immediately after spraying, when hydration processes and strength development are still incipient [19,20]. The interaction between the matrix and the percolating water induce portlandite leaching [21]. This feature increases the porosity of the matrix, favoring the ingress of aggressive agents.

Furthermore, elements produced with sprayed concrete tend to present a higher water accessible porosity than elements fabricated with poured concrete. This fact occurs due to the inclusion of air during spraying, generating a higher volume of air voids in the matrix, and to the use of accelerators [22,23], which leads to a fast setting and does not allow enough time for the matrix to consolidate properly [22,24]. In the case of discontinued flow of concrete and accelerator, or even mixing difficulties, regions of the matrix may present different porosities. Therefore, the selection of proper cement and accelerator type and dosage plays a crucial role on the durability of sprayed concrete, since it governs the development of mechanical strength at early and late ages and may affect the durability of the matrix [22,24].

Although substantial work has been conducted in the field of ESA in cement-based materials, most papers deal with conventional mortars and concretes. To illustrate this, Table 1 summarizes some of the most relevant recent studies (from 2013 to 2019) on the topic. It is possible to observe that little research is found on sprayed concrete containing accelerators and none of them deals with the influence of accelerator type and dosage on the chemical, microstructural and mechanical properties of sprayed concrete subjected to ESA. The only paper found on ESA in sprayed concrete was published by Paglia et al. [25] in 2002.

In this context, the objective of this study is to evaluate how accelerator type and dosage and the interaction between cement and accelerator influence the durability of sprayed concrete exposed to a sulfate solution. This paper represents the continuation of our previous research on sprayed concrete published in 2019 [41]. Therefore, information regarding characterization of materials and production processes of cement pastes and sprayed concrete is not fully presented here to avoid repetition.

2. Experimental methodology

This research was conducted at the Laboratory of Materials, Components and Construction Processes from the Polytechnic School of University of São Paulo and at the Laboratory of Civil Construction Engineering from São Judas Tadeu University. The scheme of the experimental program conducted is represented in Fig. 1. XRD and TGA were performed with cement pastes to avoid the dilution of phases by aggregates with the aim of quantifying phases present in small amounts (below 2% by mass) [26].

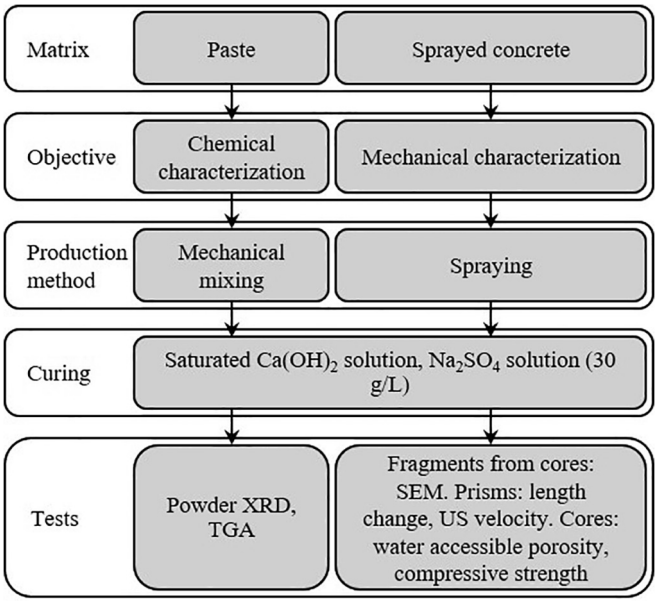

Fig. 1. Scheme of the experimental program conducted in this study.

2.1. Materials and composition of cement pastes and concrete

The cementitious material was a CEM II/B-S 42.5 R, composed by 70% CEM I 52.5 R and 30% blast-furnace slag (mass percentages), whose chemical composition obtained by XRF spectrometry is presented in Table 2. Its specific surface area determined by BET was 1.16 m^2/g and the amount of insoluble residue determined according to [42] was 1.32% by cement weight (% bcw). The mineralogical composition of this cement is shown in Table 3. It is important to mention that the crystalline phases quantified correspond to the clinker and gypsum amounts contained in cement, since the slag employed for its production is completely amorphous [41].

Distilled water, a superplasticizer based on a polycarboxylate solution (34% of solid content) and two accelerators were used to produce cement pastes. One accelerator was composed by an aluminum hydroxysulfate solution, while the other was based on a sodium aluminate solution. These accelerators were selected to cover the types commonly found in practice, following our previous publication [41]. They are identified as AF and AK, respectively, and their properties are presented in Table 4.

Cement pastes were produced using a fixed water/cement (w/c) ratio equal to 0.45 and superplasticizer at 0.70% bcw (preparation procedure described in detail in [41]). The alkaline accelerator was added at 2.0 and 4.0% bcw and the alkali-free accelerator was

Table 1
Summary of recent studies (2013–2019) on sulfate attack in cementitious matrices.

Reference	Concrete type		Characterization			Use of accelerators	Evaluation of accelerator type and dosage on sprayed concrete durability
	Conventional	Sprayed	Chemical	Microstructural	Physical / Mechanical		
[26]	•		•				
[1,18,27–29]	•		•	•			
[30–32]	•		•		•		
[2,3,33–35]	•		•	•	•		
[36]		•	•	•			
[37]		•		•	•	•	
[38–40]		•	•	•	•	•	
This study		•	•	•	•	•	•

Table 2
Chemical composition of CEM II/B-S 42.5R determined by XRF spectrometry.

Compound	LOI	CaO	SiO_2	Al_2O_3	Fe_2O_3	SO_3	MgO	K_2O	Na_2O	Minor components	Total sum
Mass percentage (%)	2.38	57.53	24.96	6.73	2.37	2.03	2.64	0.75	0.29	0.31	100.0

Table 3
Mineralogical composition of CEM II/B-S 42.5R determined by XRD/Rietveld refinement.

Compound	C_3S	C_2S	C_3A	C_4AF	CaO	$CaCO_3$	Gypsum	Hemihydrate	Amorphous phases	Total sum
Mass percentage (%)	45.9	6.2	2.9	7.5	0.3	3.7	0.8	2.0	30.7	100.0

Table 4
Properties of accelerators.

Property	AF	AK
Solid content (%)	40.0	43.0
Specific weight (g/cm^3)	1.32	1.45
pH at 20 °C	2.5	13.0
Al_2O_3 content (%)[a]	11.2	24.0
SO_3 content (%)[b]	23.0	–
Na_2O content (%)	–	19.0
SO_3/Al_2O_3 molar ratio	2.18	–
Stabilizing agent	organic acid	–

[a] Al_2O_3 corresponds to Al^{3+} and $[Al(OH)_4]^-$ in AF and AK, respectively.
[b] Sulfate ions are represented by SO_3 for convenience of the reader, since this was the representation adopted in Table 2.

employed at 6.0 and 8.0% bcw. For each sample, 150 g of paste were prepared. This amount was divided in cylindrical plastic flasks measuring 40 mm in diameter and 6 mm in height, which contained approximately 15 g of paste each. After molding, flasks were sealed and stored at 23 °C for 7 days. Then, pastes were demolded and destined to curing and to the exposure to the aggressive solution (described in Section 2.3).

The composition of each paste in terms of phases consumed and formed by accelerator reaction is presented in Table 5. The sulfate balance of accelerators is an important parameter to calculate the final SO_3/Al_2O_3 ratio of the matrix, which determines if the matrix is properly or undersulfated. This ratio may be used to predict if accelerated C_3A reactions may occur, with the consequent early formation of AFm phases [43]. Since AFm phases are directly related to the durability of cementitious matrices against ESA [7], the SO_3/Al_2O_3 ratio will be used for further discussion.

Concrete was produced using the same cementitious material, potable water and three types of siliceous aggregates (fine sand, coarse sand and gravel), whose characterization is presented in our previous paper [41]. Three different admixtures were required to produce concrete, in order to provide an adequate workability and pumpability of the fresh mix and to avoid unexpected hydration processes during its transportation from the mixing plant to the spraying site. These admixtures were a plasticizer based on a lignosulphonate solution (21% solid content), a superplasticizer based on a polycarboxylate solution (34% solid content) and a retarder composed by a sucrose derivative (28% solid content). Accelerators were the same as the ones used for cement pastes (AK and AF). It is important to mention that dispersing admixtures did not cause any deleterious processes to the matrix, as indicated in [41].

Concrete was composed by CEM II/B-S 42.5 R, fine sand, coarse sand, gravel and water, whose respective relative masses were 1.00:1.44:0.788:2.10:0.50. Plasticizer, superplasticizer and retarder were added at 0.46, 0.21 and 0.28% bcw, respectively. Fresh concrete presented a specific weight equal to 2.33 kg/m^3 and its entrapped air content was 1.5%. The dosages of accelerator AK were 2.0 and 4.0% bcw and the dosages of accelerator AF were 6.0 and 8.0% bcw. Since concretes contained the same accelerator dosages as cement pastes, their composition regarding phases consumed and formed by accelerator reaction is presented in Table 5.

Concrete was sprayed following the procedure presented in [41]. One square frustum-shaped wood panel, whose base side, top side and height measured 1000, 600 and 200 mm, respectively, was used for each mixture. Two days after spraying, 36 cylindrical specimens measuring 75 mm in diameter were drilled from each panel. Then, their extremities were cut using a diamond concrete table saw and polished using a diamond polisher to obtain a height equal to 150 mm. 32 of these specimens were destined to mechanical tests and 4 of them were cut using a diamond concrete table saw, obtaining 12 cylindrical specimens measuring 75 mm in diameter and 50 mm in height, which were destined to the determination of water accessible porosity. To finalize, 10 prismatic specimens measuring 25 mm in height, 25 mm in width and 250 mm in length were cut using a diamond concrete table saw from the parts of the concrete panels remaining after the extraction of cylindrical specimens.

Pastes and concretes that do not contain accelerators are identified as *'REF'*, while matrices produced with accelerators are named by *'accelerator name and dosage'*. Concrete REF (with no

Table 5
Composition of cement pastes.

Phase/compound	REF	AF 6%	AF 8%	AK 2%	AK 4%
Total SO_3 in cement (mmol/g cement)	25.29	25.29	25.29	25.29	25.29
Al_2O_3 in accelerator (mmol/g cement)	–	6.59	8.79	4.71	9.42
SO_3 in accelerator (mmol/g cement)	–	17.24	22.98	0.00	0.00
AFt formed by accelerator reaction (mmol/g cement)[a]	–	6.59	8.79	4.71	8.43
AFm formed by accelerator reaction (mmol/g cement)[b]	–	–	–	–	0.98
SO_3 consumed by accelerator reaction (mmol/g cement)	–	19.77	26.36	14.12	25.29
SO_3 left after accelerator reaction (mmol/g cement)	25.29	22.76	21.92	11.17	0.00
Final SO_3/Al_2O_3 molar ratio[c]	0.38	0.34	0.33	0.17	0.00

[a] Calculated considering that Al_2O_3 from accelerator is totally consumed to form AFt (SO_3 is not the limiting reactant).
[b] Calculated considering the amount of Al_2O_3 from accelerator that remained after all the sulfate was consumed to form AFt (SO_3 as the limiting reactant to form AFt).
[c] Calculated considering the sulfate amount remaining after accelerator reaction and the initial Al_2O_3 content of cement.

accelerator) was also produced by spraying, positioning the mold horizontally to avoid sagging.

2.2. Sulfate solution

The main salts associated to ESA are calcium, magnesium and sodium sulfates, whose solubilities in water at 20 °C provide sulfate concentrations equal to 0.015 mol/L, 1.1 mol/L and 1.97 mol/L, respectively [44]. According to EN 206-1 [45], the sulfate concentration equal to 3 g/L is the upper limiting value of the moderately aggressive exposure class for concretes subjected to chemical attack. As calcium sulfate provides 1.44 g of sulfates per liter, a significant reduction in the rate of degradation caused by ESA would occur. In addition, since Mg^{2+} replaces Ca^{2+} in the structure of hydrated silicates forming non-cementing phases [46], sodium sulfate was used in this study.

Since leaching is the driving force that triggers sulfate attack, it is necessary to increase sulfate concentration to obtain a faster degradation [8]. Therefore, the concentration of the sodium sulfate solution employed was 30 g/L, which was based on a series of previous works [8,14,30,47,48]. In addition to that, this is the reference concentration for the evaluation of ESA in sprayed concrete [20].

2.3. Curing and exposure to sulfate solution

All paste and sprayed concrete specimens were cured by immersion in a saturated $Ca(OH)_2$ solution for 7 days after their production. At that age, half of the specimens of each composition was kept in the saturated $Ca(OH)_2$ solution. These specimens were the reference for comparative purposes. The other half of specimens was transferred to a Na_2SO_4 solution with the concentration of 30 g/L. In both cases, the volume ratio solution/specimen was 10 (solution to surface ratio equal to 50 L/m^2), based on [49].

350 L-containers employed to store specimens were filled with the solution up to their top and covered to reduce contact with air and CO_2 dissolution. Three water pumps PH-101 (flow rate equal to 150 L/h) were used to ensure a continuous flow of solution inside each container. Solutions were renewed once a month, which should be representative of field conditions, where concrete is exposed to continuous supply of sulfate ions [1]. The pH of the sodium sulfate solution was measured weekly and the values obtained were within the interval (10.6 ± 0.2).

2.4. Test methods

Table 6 shows the tests performed in this study. Their descriptions are presented subsequently. The immersion of the specimens in the Na_2SO_4 solution was considered as 'time 0' for all the tests.

2.5. Powder XRD

Powder XRD was performed to determine the phase composition of cement pastes at 7, 28, 91 and 270 days of sulfate exposure. At these ages, pastes were washed in distilled water, dried using the solvent exchange method with isopropanol and diethyl ether [41,56] and ground to a maximum particle size of 63 μm using an agate mortar. Tests were conducted using the same parameters described in [41]. Phase structures for Rietveld refinement using the external standard method are indicated in [23,41].

2.6. Thermal analysis

TGA was performed from 25 to 1000 °C at a heating rate of 10 °C/min with N_2 flow of 60 mL/min using a Netzsch Libra 209 F1 thermobalance. Tests were conducted with the same samples produced for powder XRD, in order to normalize the results from Rietveld refinement by cement content. In each analysis, approximately 50 mg of paste were tested in 90 μL open alumina crucibles.

The mass loss corresponding to the release of CO_2 due to the decarbonation of $CaCO_3$ was calculated from 550 to 750 °C. The amount of chemically bound water was determined by the mass loss from 25 to 1000 °C, subtracted by the mass of CO_2 contained in carbonated phases.

2.7. Scanning electron microscopy

Scanning electron microscopy was performed to analyze the microstructure of the sprayed concrete subjected to ESA at 28, 91 and 270 days. Tests were executed in a Quanta FEG 650 microscope at the voltage of 20 kV. After the determination of compressive strength, concrete fragments were detached from the surface of cores that was in contact with the solution. The fracture zone was analyzed perpendicularly to the surface of the specimen, until a depth of 5 mm. Samples were dried by the solvent exchange method [41,56], similarly to XRD analyses, and coated with carbon. Morphology of the precipitated hydrates was evaluated by secondary electron imaging and their chemical composition was assessed by energy dispersive X-ray analysis.

2.8. Length change

Unrestrained length change was monitored to evaluate how ESA affects the dimension stability of sprayed concrete until the age of 270 days, adapting the procedures described in [53]. Prismatic specimens were sawn from sprayed concrete panels. Their base measured 25 × 25 mm and their length was 250 mm. Two stainless steel pins were glued using an epoxy adhesive to one face of the specimens with a distance of 150 mm between them to serve as reference points [26]. The length variation was measured in a length comparator. Five specimens were tested for each mix composition immersed in the $Ca(OH)_2$ and Na_2SO_4 solutions.

2.9. Determination of US propagation velocity

US propagation velocity was determined to analyze the rate of deterioration of the microstructure of sprayed concrete during sulfate exposure, until the age of 270 days. This test was performed in

Table 6
Tests performed to evaluate the durability of sprayed concrete against ESA.

Matrix	Test	Specimen	Age/period	Reference
Cement paste	Powder XRD	Ground hardened paste	7, 28, 91 and 270 days	[50]
	Thermal analysis	Ground hardened paste	7, 28, 91 and 270 days	[51]
Sprayed concrete	SEM	Fragments derived from cores	28, 91 and 270 days	[52]
	Length change	Sawn prisms	Weekly, until 270 days	[53]
	Determination of US propagation velocity	Sawn prisms	Weekly, until 270 days	[20]
	Water accessible porosity	Extracted cores	28, 91, 182 and 270 days	[54]
	Compressive strength	Extracted cores	28, 91, 182 and 270 days	[55]

the prismatic specimens used for the determination of length variation. A direct longitudinal reading was obtained using a CNS PUNDIT LAB+ equipment, coupled with 200 kHz transducers. Five specimens were tested for each mix composition immersed in each solution.

2.10. Water accessible porosity

Water accessible porosity (W_p) was determined according to [54] with concrete cores measuring 75 mm in diameter and 50 mm in height extracted from sprayed panels, immersed in the $Ca(OH)_2$ and Na_2SO_4 solutions. At the ages of 28, 91, 182 and 270 days, specimens were removed from the solutions and washed with water. Their saturated weight (w_s) was measured after that. Then, specimens were dried at 60 °C for five days and their dry weight (w_d) was determined. This temperature was used in order to avoid dehydration of C-S-H and ettringite. Water accessible porosity was calculated using Eq. (1). Three specimens were tested at each age for all mix compositions immersed in the $Ca(OH)_2$ and Na_2SO_4 solutions.

$$W_p = 100\hat{A} \cdot \frac{w_s - w_d}{w_d} \quad (1)$$

2.11. Determination of compressive strength

Compressive strength was determined in cylindrical cores measuring 75 mm in diameter and 150 mm in height immersed in the $Ca(OH)_2$ and Na_2SO_4 solutions to analyze how ESA influences the mechanical strength of sprayed concrete. Tests were conducted in a Shimadzu Universal Testing Machine, model UH-F1000 kN, at a loading rate equal to 0.45 MPa/min, according to [55]. Four specimens were tested for each mix composition immersed in the $Ca(OH)_2$ and Na_2SO_4 solutions at the ages of 28, 91, 182 and 270 days.

3. Results and discussion

3.1. Powder XRD

Fig. 2 depicts the evolution of phase composition in cement pastes determined by powder XRD until 270 days of sulfate exposure. These results were normalized by cement weight, considering the amount of chemically bound water of each sample determined by TGA. In order to simplify the interpretation of results, only the crystalline phases that interact with sulfate ions are presented (portlandite, gypsum, AFm phases and ettringite). Results obtained with pastes immersed in the saturated calcium hydroxide solution are grouped on the left, while results from pastes immersed in the sodium sulfate solution are grouped on the right.

In Fig. 2a, a reduction in portlandite content is observed, despite using a saturated calcium hydroxide solution for curing. The main cause of this reduction is that the quantification by XRD/Rietveld refinement is based on the sample mass, which is composed by crystalline and amorphous phases. As hydration progresses, the amount of amorphous phases increases significantly (from 30% at 24 h to almost 70% at 270 days). Even expressing the result normalized by cement weight, a reduction in the amount of crystalline phases is observed, as is the case of portlandite. In addition, containers used to store specimens were not airtight, which led to carbonation of calcium hydroxide in solution and, therefore, a slight reduction in portlandite may have occurred due to that process.

In pastes immersed in the sodium sulfate solution (Fig. 2b), portlandite contents tend to decrease faster than in pastes immersed in the calcium hydroxide solution due to the dissolution and leaching of this phase. This occurs because the sodium sulfate solution does not contain calcium ions, favoring portlandite dissolution in order to meet the thermodynamic condition for equilibrium of that ion in solution.

Furthermore, portlandite reacts with sulfate ions in solution, forming gypsum [21]. This may be observed in Fig. 2d, where gypsum is formed in pastes immersed in the sodium sulfate solution. Initial gypsum formation is more pronounced in pastes containing accelerators than in paste REF because the use of accelerators increases the porosity of the matrix, facilitating sulfate ingress. Gypsum contents tend to increase until 28 days and decrease after that. Notice that no gypsum was found in pastes immersed in the calcium hydroxide solution (Fig. 2c), which agrees well with thermodynamic data obtained by [57].

Gypsum is a metastable product because it is formed by sulfate ingress and leads to the conversion of AFm phases into ettringite. Analyzing Fig. 2e and f, pastes immersed in the sodium sulfate solution present lower contents of AFm phases at 7 days when compared to pastes immersed in the calcium hydroxide solution. In Fig. 2.f, it is possible to see that AFm consumption from zero to 28 days follows the descending order AK 4% > AK 2% > AF 8% > AF 6% (reductions equal to 88%, 67%, 17% and 16% for pastes AK 4%, AK 2%, AF 8% and AF 6%, respectively). AFm consumption follows the inverse order of the final SO_3/Al_2O_3 ratio of the paste.

As expected, Rietveld quantification reveals increasing amounts of ettringite in pastes immersed in the sodium sulfate solution (Fig. 2h). Ettringite is formed by the reaction of AFm phases with gypsum and Ca^{2+} and OH^- ions derived from portlandite dissolution. Results show that ettringite formation depends on accelerator type and dosage. The higher the aluminum content incorporated by accelerator (AK 4% > AF 8% > AF 6% > AK 2%, Table 5), the larger the ettringite amount formed by sulfate ingress (Fig. 2h). The increase in ettringite contents from zero to 28 days is equal to 16%, 11%, 6% and 5% for pastes AK 4%, AK 2%, AF 8% and AF 6%, respectively. Ettringite formation follows the same order as AFm consumption and the inverse order of the final SO_3/Al_2O_3 ratio of the paste.

3.2. Scanning electron microscopy

Fig. 3 presents SEM images obtained with sprayed concrete REF at 28, 91 and 270 days. Fig. 3a, c and e represent samples cured in the saturated calcium hydroxide solution (grouped on the left) and Fig. 3b, d and f represent samples immersed in the sodium sulfate solution (grouped on the right). Figs. 4 and 5 present the microstructure of concretes AF 8% and AK 4% and are organized the same way as Fig. 3. Regions analyzed by EDS are indicated by a number in the corresponding image. Results obtained in the EDS spectra are represented as the relative molar amounts of each element, placed above each image.

In Fig. 3a, c and e, SEM images of concretes REF immersed in the $Ca(OH)_2$ solution are shown. Pores measuring 50–100 μm in diameter are observed, where plate-like crystals are deposited. These crystals may represent AFm phases according to the EDS results from Fig. 3c, which indicate an Al/S ratio higher than 1.

The formation of secondary sulfate phases by ESA changes the microstructure of the matrix. Concrete REF immersed in the sodium sulfate solution at 28 days (Fig. 3b) presents needle-like crystals precipitated in the pore. These crystals are identified as ettringite, considering their morphology and composition determined by EDS (Al/S ratio equal to 0.7). At 91 days (Fig. 3d), the amount of phases precipitated in the pore increased due to the progress of sulfate attack. These phases are composed mainly of AFm and ettringite (Al/S ratio between 0.9 and 1). At 270 days (Fig. 3f), the pore presents an elevated quantity of ettringite (Al/S ratio = 0.70). This sequence of analysis indicates that the ingress

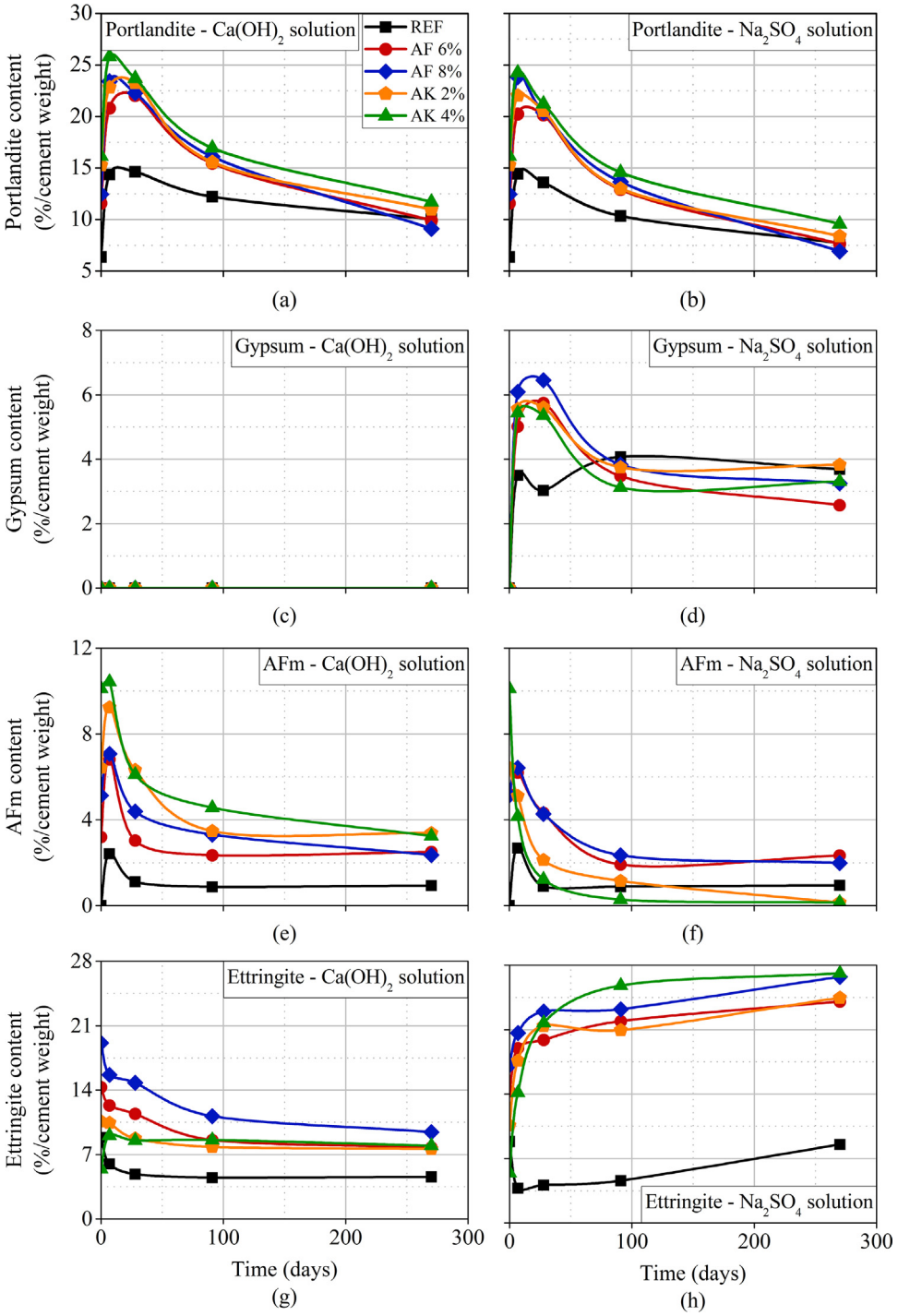

Fig. 2. Evolution of portlandite (a and b), gypsum (c and d), AFm phases (e and f) and ettringite (g and h) contents in pastes immersed in saturated calcium hydroxide solution (left) and sodium sulfate solution (right) until 270 days.

of external sulfates transforms AFm phases into ettringite, as expected.

It is also remarkable that the morphology of crystals precipitated in the pore changes as external sulfate attack progresses. At 28 days, well-defined needle-like crystals measuring 15 μm in length are uniformly distributed, growing perpendicularly to the surface of the pore. However, at 91 and 270 days, pores are filled by ball-shaped clusters measuring around 10 μm in diameter, formed by the agglomeration of needle-like crystals around 5 μm-long. This analysis indicates that crystals precipitated initially are formed at a slower rate, when the pore is not supersaturated with sulfate ions. As external sulfate ingresses in the matrix, poorly crystalized ettringite clusters form due to the supersaturation of the aqueous solution in sulfate ions. This fact was also observed by [1].

In concretes AF 8% and AK 4% (Figs. 4 and 5, respectively), pores are larger than in concrete REF, measuring around 150–200 μm in diameter. This occurs due to the use of accelerators, which lead to a fast setting and do not allow enough time for the matrix to consolidate properly [22,24]. In addition, since accelerators contribute to

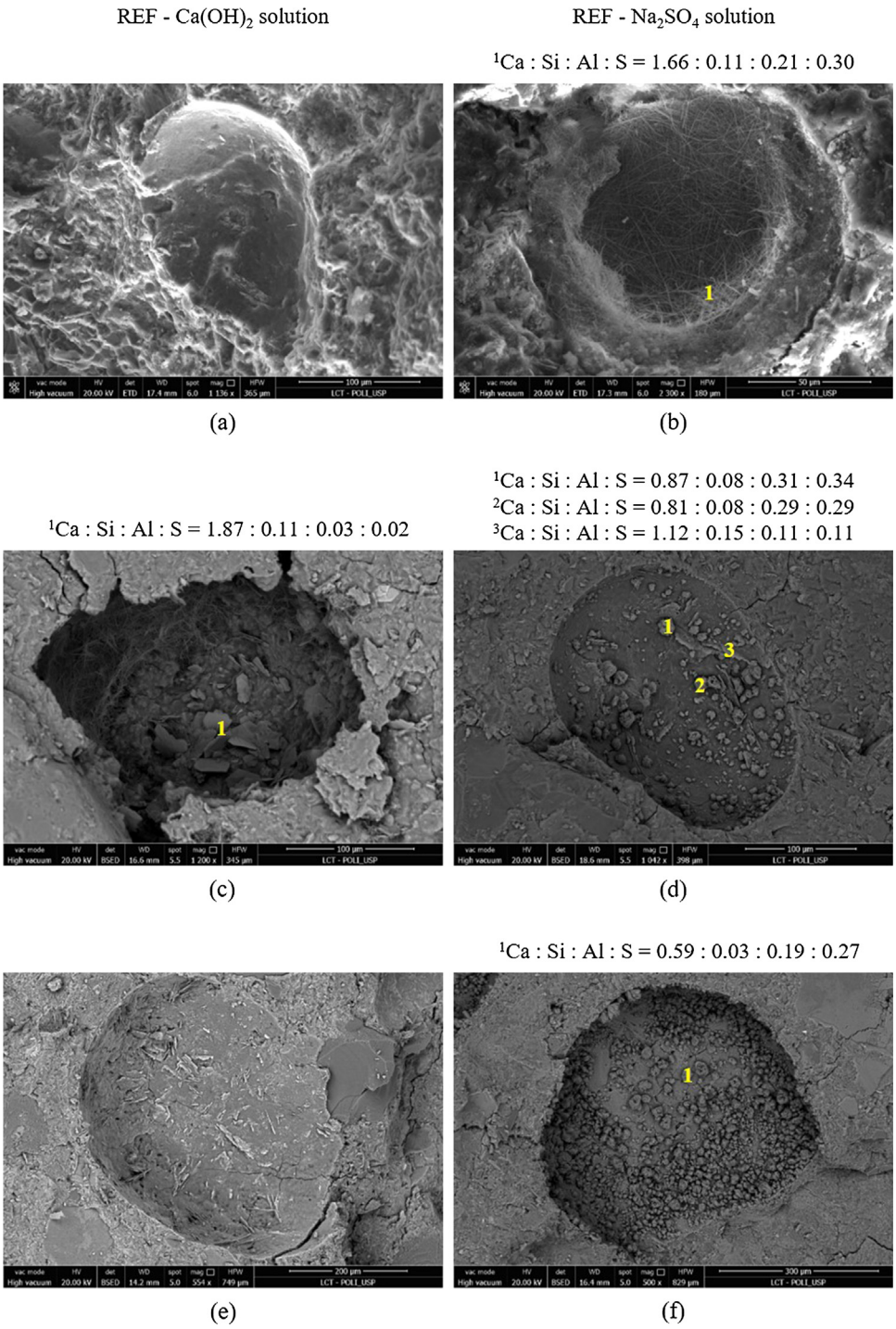

Fig. 3. SEM images of sprayed concrete REF immersed in the calcium hydroxide solution at 28 (a), 91 (c) and 270 days (e) and immersed in sodium sulfate solution at 28 (b), 91 (d) and 270 days (f).

increase the content of aluminate hydrates in the matrix, the amount of plate-like crystals found inside the pores of concretes AF 8% (Fig. 4a) and AK 4% (Fig. 5a) immersed in the calcium hydroxide solution is larger than in concrete REF (Fig. 3a). As hydration progresses, the amount of AFm phases inside the pores increases (Fig. 4c, 4e, 5c and 5e), due to the constant hydration reactions of C_3A and C_4AF.

As concretes produced with accelerators contain more AFm phases than concrete without accelerator, the content of ettringite precipitated in the pores of AF 8% and AK 4% seems to be higher than in concrete REF, as may be observed in Fig. 4b and 5c. At 28 days, ettringite is formed as needle-like crystals measuring around 15 μm in length. This occurs similarly to concrete REF, where crystals are formed at a slower rate because pores are not supersaturated with sulfate ions.

As ESA progresses and the pore solution becomes supersaturated with sulfate ions, ettringite clusters form, as may be observed in Fig. 4d, 4f, 5d and 5f. At 91 days, ettringite clusters formed in concrete AF 8% (Fig. 4d) and AK 4% (Fig. 5d) present a diameter equal to 15 μm, which are larger than in concrete REF (Fig. 3d).

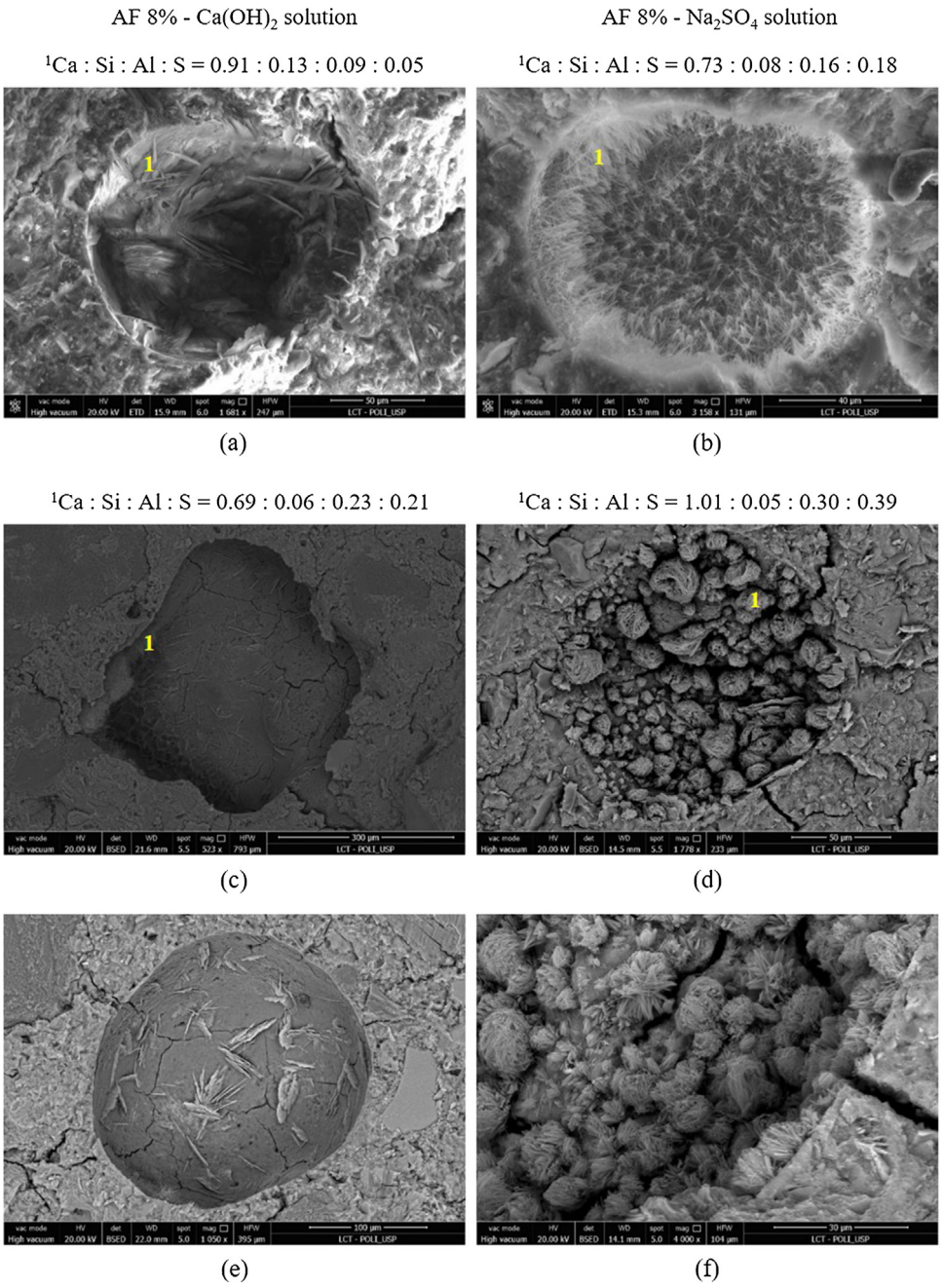

Fig. 4. SEM images of sprayed concrete AF 8% immersed in the calcium hydroxide solution at 28 (a), 91 (c) and 270 days (e) and immersed in sodium sulfate solution at 28 (b), 91 (d) and 270 days (f).

In addition, pores present a denser precipitation of ettringite clusters in concretes produced with accelerators. At 270 days (Fig. 4f and 5f), the same tendency is observed, densifying the pores with the precipitation of ettringite clusters.

3.3. Determination of length change and US propagation velocity

Fig. 6 shows images of prismatic specimens subjected to ESA. Fig. 6a and b depict specimens of concrete AK 4% after 147 days of immersion in the sodium sulfate solution, which were severely degraded at that age. Some specimens cracked near the edges, which presented a high degree of damage. Cracks in the transversal direction caused an early failure of the specimens.

A specimen of concrete AF 8% after 270 days of sulfate exposure is presented in Fig. 6c. A slight crack at the borders is observed, with no transversal cracks. Visual inspection of concretes AF 6%, AK 2% and REF indicates no major failure in the form of spalling of the external surface, generalized cracking or tensile splitting of the specimens.

Edge cracking is usually the first visual consequence of ESA since it is associated to an intensification effect of sulfate penetration combined with a low material restrain in those regions. Cracking of the cross section and longitudinal cracking are serious failure modes caused by the interaction between the sound core of the specimen and the external layers directly affected by sulfate penetration. Such deterioration is caused by the conversion of AFm phases into ettringite due to the ingress of sulfate ions in the

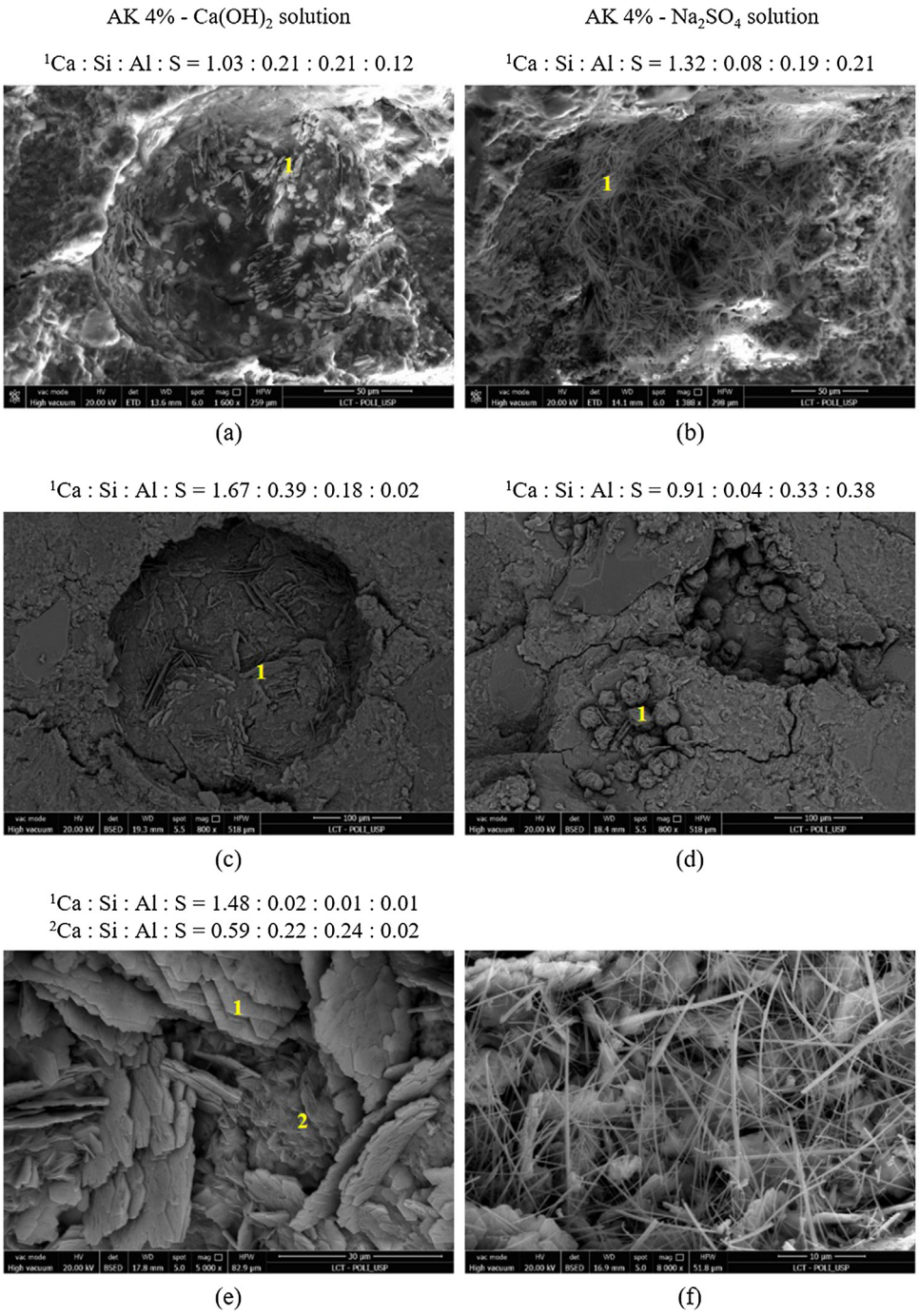

Fig. 5. SEM images of sprayed concrete AK 4% immersed in the calcium hydroxide solution at 28 (a), 91 (c) and 270 days (d) and immersed in sodium sulfate solution at 28 (b), 91 (d) and 270 days (f).

matrix. Differences observed between concretes AK 4% and AF 8% may be corresponded to the larger amount of AFm phases produced by accelerator reaction when AK is employed (Fig. 2), which leads to a matrix more prone to suffer the effects of sulfate attack.

Fig. 7 presents the average values of length change and US propagation velocity of prismatic specimens until 270 days. Results obtained with specimens immersed in the saturated calcium hydroxide solution are grouped on the left, while results from specimens immersed in the sodium sulfate solution are grouped on the right. Concrete AK 4% failed at the age of 147 days and, therefore, readings with those specimens were discontinued.

As may be observed in Fig. 7a, specimens immersed in the saturated $Ca(OH)_2$ solution present an expansion until 20 days, approximately, which may be associated to the ingress of water in the specimens. After that, specimens start to shrink due to the progress of cement hydration (autogenous shrinkage). The hydration progress may also be correlated with the increase in the US propagation velocity observed in Fig. 7c. The initial sharp increase in US velocity until 10 days is associated with the ingress of water in the pores, which facilitates US propagation. As hydration advances, pores are filled with hydrated phases, densifying the matrix and reducing the obstacles for the propagation of US waves, increasing its velocity [24].

Fig. 6. Specimens of concrete AK 4% after 147 days of sulfate exposure (a and b) and concrete AF 8% after 270 days of sulfate exposure.

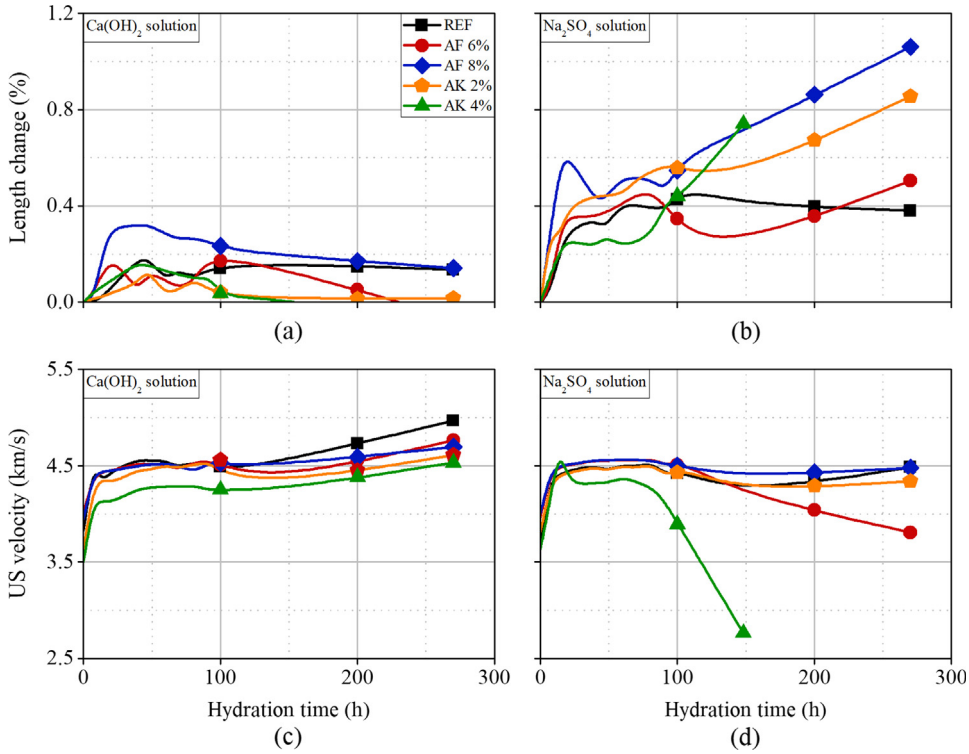

Fig. 7. Length change (a and b) and US propagation velocity (c and d) of sprayed concrete immersed in the saturated $Ca(OH)_2$ solution (left) and in the Na_2SO_4 solution (right) until 270 days.

Analyzing specimens subjected to ESA (Fig. 7b), the initial expansion until 20 days caused by the immersion in the sodium sulfate solution is also observed. It is more intense than in specimens immersed in the calcium hydroxide solution due to the high initial sulfate concentration gradient between solution outside and inside the specimen, which facilitates sulfate ingress in the matrix. Expansions in specimens subjected to ESA are caused by the crystallization pressure exerted on the pore walls due to the formation of ettringite, which precipitates from a sulfate supersaturated solution in confined conditions and convert the chemical energy into mechanical work [58,59].

Expansions and deterioration occur at a larger extent in sprayed concrete containing accelerators because the additional aluminum content incorporated makes the matrix more vulnerable to ESA [60]. Concrete REF reaches it maximum expansion at 100 days and starts to shrink after that. On the contrary, all concretes produced with accelerators develop different degrees of expansion during the attack, ranging from 8 to 11.5 mm/m at the age of 270 days. From the samples that did not fail until 270 days, the highest expansion value was obtained with concrete AF 8%, which reached 11.5 mm/m at 270 days.

This may be explained because this accelerator used at 8% bcw provides the highest aluminum concentration (Table 5), which leads to the largest amount of ettringite formed during ESA (Fig. 2h). In addition, AF 8% promotes the fastest setting [41], which leads to an improper consolidation of the matrix, increasing its porosity [22]. Although the higher porosity facilitates sulfate ingress, it increases the capacity of the matrix to accommodate

the precipitated expansive phases [27]. Therefore, concrete AF 8% does not fail, although it contains a similar ettringite content to AK 4% at 270 days (Fig. 2h).

Kinetics of specimen expansion from 80 days on depends on accelerator type and dosage and follows the descending order AK 4% > AK 2% > AF 8% > AF 6% > REF, which is the inverse order of the final SO_3/Al_2O_3 ratio of the matrix (Table 5). The highest expansion rate was observed with concrete AK 4%, which expanded 4.7 mm/m from 80 to 147 days and presented early fracture. This occurs because accelerator AK does not contain sulfates in its formulation (Table 4). Concrete AK 4% presented the lowest SO_3/Al_2O_3 molar ratio (Table 5) and contained the largest amount of AFm phases formed by accelerator reaction, turning the matrix more susceptible to the effects of ESA.

The effects of sulfate ingress may also be observed by the US propagation velocity. Variations in US velocity may be correlated to changes in the density and integrity of the specimens. Positive increments suggest denser matrices and negative variations indicate the occurrence of damages. The resulting value obtained for US velocity corresponds to the combined effect of these two processes. If US velocity increases, ettringite precipitation prevails over matrix cracking, whereas if US velocity decreases, cracking is more important than ettringite formation. If US velocity is maintained constant, it may be concluded that the densification caused by ettringite precipitation is counterbalanced by the deleterious effect of matrix cracking.

The initial US velocity until 20 days increases quickly due to the ingress of water in the matrix, as also observed in the specimens immersed in the saturated $Ca(OH)_2$ solution. From 20 to 80 days, US velocity increases slightly for concretes AF 6%, AF 8% and AK 2% due to the deposition of ettringite crystals in the pores. During this stage, ettringite precipitation prevails over the micro-cracking caused by the ingress of sulfates. From 80 days on, US velocity starts to decrease, which is associated with damages and microcracking caused by ettringite formation. These damages act as obstacles for US propagation, decreasing its velocity. After 150 days, concretes AF 8% and AK 2% present a slight increase in US velocity, which may be associated with the precipitation of ettringite in the pores, densifying the matrix and facilitating US propagation.

The most severe case is observed with concrete AK 4%, as also observed by length change measurements. The formation of damages in the matrix starts the earliest, at around 20 days, where a significant drop in US velocity is observed. From 30 to 60 days, US velocity increases slightly due to ettringite precipitation. After that, US velocity decreases sharply, which is associated with the complete failure of the specimens (Fig. 6a). These results are in total agreement with the length change measured in concrete AK 4% (Fig. 7b) and indicate that the sprayed concrete produced with alkaline accelerators tend to be more vulnerable to the deleterious effects of ESA.

3.4. Water accessible porosity

Fig. 8 depicts the average values of water accessible porosity of concrete cores immersed in the saturated calcium hydroxide solution (Fig. 8a) and in the sodium sulfate solution (Fig. 8b) at the ages of 28, 91, 182 and 270 days. A significant difference in water accessible porosity in concrete with and without accelerators is observed (Fig. 8a). Concrete REF presents the lowest values of water accessible porosity at all the ages analyzed.

Concretes produced with accelerators present higher values of water accessible porosity due to the fast setting caused by accelerators which caused an improper consolidation of the matrix. Water accessible porosity is directly proportional to accelerator reactivity, that is, the faster the setting accelerator promotes [41], the higher the water accessible porosity of the matrix. The descending order of water accessible porosity is AF 8% > AF 6% > AK 4% > AK 2% > REF. This occurs because the fast setting does not allow enough time for the matrix to consolidate properly and eliminate the entrapped air, leading to higher porosities. As observed in Figs. 4 and 5, pores measuring around 150–200 μm in diameter are observed in sprayed concretes.

As hydration progresses, all concretes analyzed experience a reduction in water accessible porosity, as expected. A reduction of 30% is observed in concrete REF from 28 to 270 days, while a reduction between 8 and 17% is observed in concretes containing accelerators. This behavior may be explained by the suppress in alite hydration in accelerated matrices [43], limiting the formation of hydrated products and consequently the filling of pores.

Analyzing the samples immersed in the sodium sulfate solution (Fig. 8b), concrete REF presents a reduction in water accessible porosity until 182 days, which may be associated to pore filling caused by the hydration progress and by ettringite formation. From 182 to 270 days, a slight increase is observed, indicating that some damage may have been caused by ESA.

This analysis becomes clearer with respect to concretes produced with accelerators. Concretes AF 6% and AF 8% present a reduction in water accessible porosity until 182 days and an increase after that, similarly to concrete REF. The porosity of concrete AK 2% decreases until 91 days and increases from 91 to 270 days. Concrete AK 4% only presents increases in porosities in all ages analyzed, indicating that the damage caused by ESA and ettringite formation prevails over hydration progress. Therefore, this concrete is the most vulnerable to be damaged by the ingress of sulfate. This discussion is in total agreement with the length change results presented in Section 3.3.

3.5. Determination of compressive strength

Fig. 9 shows images of concrete cores subjected to ESA. A core of concrete AK 4% after 182 days of immersion in the sodium sulfate solution is presented in Fig. 9a and a core of concrete AF 8% after 270 days of sulfate exposure is shown in Fig. 9b.

As observed with prismatic specimens (Fig. 6), concrete cores also present damage caused by the immersion in the sodium sulfate solution. Cores of concrete AK 4% presented a severe degradation on their surface, with superficial cracks and spalling, at the age of 182 days (Fig. 9a). Cores of concrete AF 8% presented only a small spalling at the circumferential edges of the specimen after 270 days of sulfate exposure (Fig. 9b). Such degradation is associated with ettringite formation due to ESA, which is more aggressive in the matrix with the largest amount of AFm phases (AK 4%, Table 5). This deterioration may affect the mechanical properties of the matrix negatively.

Fig. 10 depicts the results of compressive strength of concrete cores at 28, 91, 182 and 270 days. Fig. 10a represents specimens immersed in the calcium hydroxide solution and Fig. 10b cores immersed in the sodium sulfate solution. It was not possible to determine the compressive strength of concrete AK 4% immersed in the sulfate solution at 182 and 270 days accurately because specimens were severely damaged and presented spalling, as observed in Fig. 9. It is important to mention that prismatic specimens presented an early fracture at 147 days, as observed in Fig. 7.

As observed in the evaluation of mechanical properties at 1 day [41], compressive strength varies significantly in concretes with and without accelerators, considering the curing in the saturated $Ca(OH)_2$ solution. For a certain age, compressive strength of concrete REF is always higher than in concretes produced with accelerators. At 270 days, concrete REF presents a compressive strength around 70% higher than concretes produced with accelerators. Since compressive strength is inversely proportional to porosity

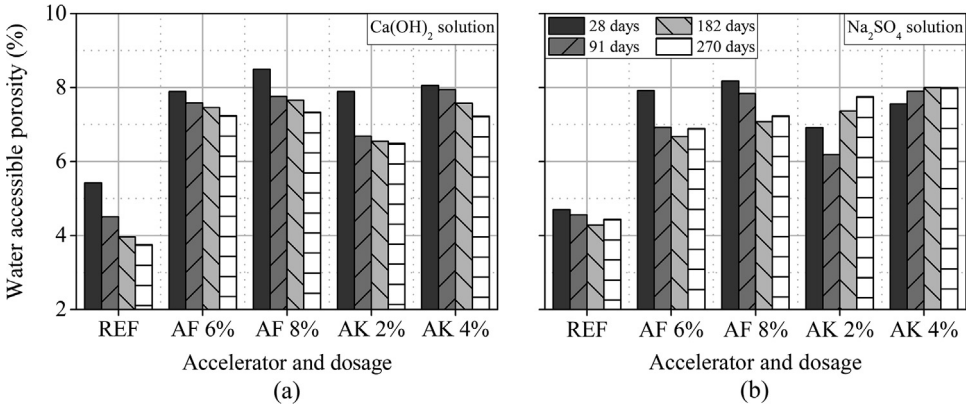

Fig. 8. Average values of water accessible porosity in sprayed concrete immersed in the saturated $Ca(OH)_2$ solution (a) and in the Na_2SO_4 solution (b) at 28, 91, 182 and 270 days.

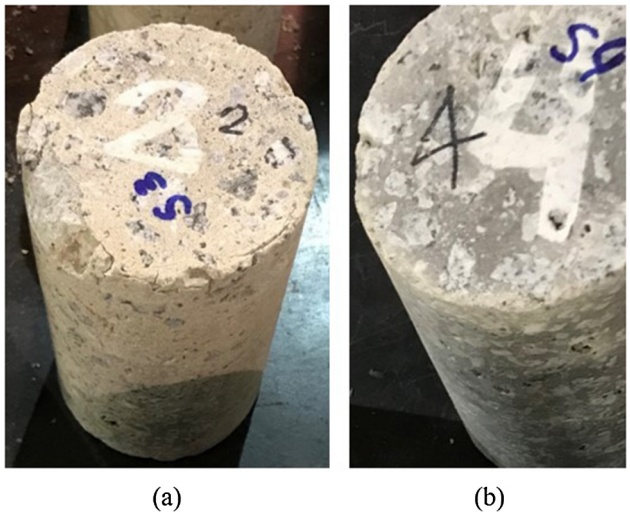

Fig. 9. Cores of concrete AK 4% after 182 days of sulfate exposure (a) and AF 8% after 270 days of sulfate exposure (b).

[61], the use of accelerators causes a reduction in mechanical strength due to the poorer consolidation of the matrix [22].

Analyzing samples immersed in the sodium sulfate solution (Fig. 10b), compressive strength of concrete REF increases until 182 days due to cement hydration progress. From 182 to 270 days, compressive strength reduces, which may be associated with damages caused by ettringite formation due to the ingress of sulfates. These results are in total agreement with the values of water accessible porosity observed in Fig. 8b.

Compressive strength of concretes produced with accelerators increases until 91 days and decreases after that. The initial increase occurs due to the cement hydration progress and the reduction is associated with the deterioration of the matrix caused by ESA. The incorporation of accelerators contributes to increase the aluminum content in the matrix and, therefore, turns it more susceptible to deteriorate when sulfate ions ingress. That effect is more evident when accelerator AK is used, because it does not contain sulfates in its formulation, which contributes to increase the amount of AFm phases in the matrix (Fig. 2). Concrete AK 4% presents the lowest compressive strength (50% lower than concrete REF at 270 days), which is in line with the results of length change (Fig. 7b). At 270 days, compressive strength follows the ascending order AK 4% < AK 2% < AF 8% < AF 6% < REF, which is the same ascending order as the SO_3/Al_2O_3 ratio of the matrix.

4. Conclusions

The following conclusions may be drawn from the results obtained in this experimental program:

Sprayed concrete produced with accelerators presented a lower durability against ESA than concretes that do not contain accelerators.

The immersion of concrete in the sodium sulfate solution induces portlandite leaching and gypsum formation, which leads to AFm conversion into ettringite.

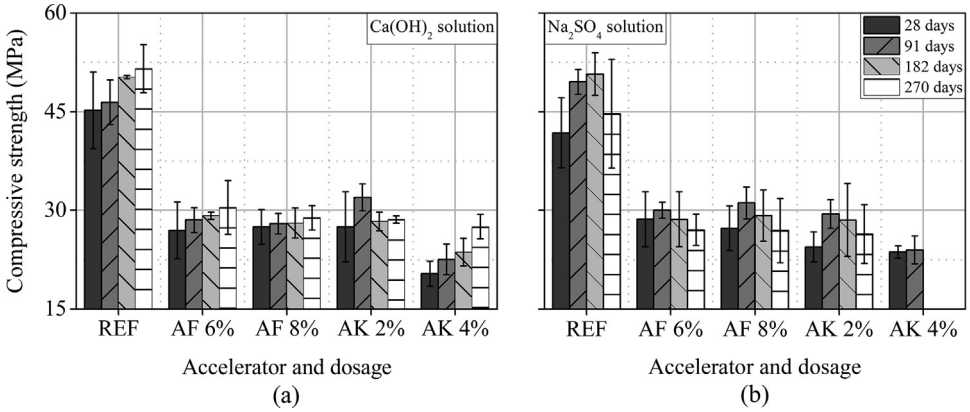

Fig. 10. Compressive strength of sprayed concrete immersed in the saturated $Ca(OH)_2$ solution (a) and in the Na_2SO_4 solution (b) at 28, 91, 182 and 270 days.

Ettringite formation occurs at a larger extent when accelerators are employed. The higher the accelerator dosage, the larger the ettringite amount formed by ESA. Reaction rates of AFm consumption and ettringite formation follow the descending order AK 4% > AK 2% > AF 8% > AF 6% > REF, which is the inverse order of the final SO_3/Al_2O_3 ratio of the paste.

Sprayed concrete containing accelerators presents pores measuring 150–200 μm in diameter, which are filled with AFm phases. Due to ESA, ettringite needle-like crystals precipitate perpendicularly to the pore surface. As ESA progresses, ettringite ball-shaped clusters measuring around 10 μm in diameter are formed by the agglomeration of needle-like crystals.

Accelerator AK leads to the fastest ettringite precipitation rate because pastes produced with this accelerator contain the largest amount of AFm phases.

Sprayed concrete containing accelerators present high expansions due to ESA, reaching from 8 to 11.5 mm/m at the age of 270 days. The higher the aluminum content of accelerator, the higher the expansion and deterioration observed and the higher the vulnerability of the matrix to ESA.

Specimen expansion rate from 80 days on follows the descending order AK 4% > AK 2% > AF 8% > AF 6% > REF, which is the inverse order of the final SO_3/Al_2O_3 ratio of the matrix. Concrete AK 4% presents the highest expansion rate and early fractures occur because this accelerator does not contain sulfates in its formulation and leads to the largest amount of AFm phases.

Compressive strength decreases as ESA progresses due to damages caused by ettringite formation. The value of compressive strength follows the ascending order AK 4% < AK 2% < AF 8% < AF 6% < REF, which is the same ascending order as the SO_3/Al_2O_3 ratio of the matrix. The most severe case is observed with concrete AK 4%, whose AFm phases content is the highest.

CRediT authorship contribution statement

Renan P. Salvador: Conceptualization, Methodology, Formal analysis, Investigation, Resources, Writing - original draft, Funding acquisition. **Dimas A.S. Rambo:** Formal analysis, Writing - original draft. **Roberto M. Bueno:** Investigation. **Silvio R. Lima:** Investigation. **Antonio D. Figueiredo:** Conceptualization, Resources, Writing - review & editing, Funding acquisition.

Declaration of Competing Interest

The authors declare that they have no known competing financial interests or personal relationships that could have appeared to influence the work reported in this paper.

Acknowledgements

The first author would like to thank FAPESP, Brazil; (Fundação de Amparo à Pesquisa do Estado de São Paulo, São Paulo, Brazil, process 2017/00125-9) for the scholarship granted. Authors thank São Judas Tadeu University for financial support. Thanks are extended to Solotrat and Concreto Projetado do Brasil for lending equipment and offering technical support, Sika for providing admixtures and Lafarge-Holcim for providing concrete. We also thank CAPES, Brazil (Coordenação de Aperfeiçoamento de Pessoal de Nível Superior).

References

[1] T. Ikumi, I. Segura, S.H.P. Cavalaro, Influence of early sulfate exposure on the pore network development of mortars, Constr. Build. Mater. 143 (2017) 33–47, https://doi.org/10.1016/j.conbuildmat.2017.03.081.

[2] C. Yu, W. Sun, K. Scrivener, Degradation mechanism of slag blended mortars immersed in sodium sulfate solution, Cem. Concr. Res. 72 (2015) 37–47, https://doi.org/10.1016/j.cemconres.2015.02.015.

[3] A. Baldermann, M. Rezvani, T. Proske, C. Grengg, F. Steindl, M. Sakoparnig, C. Baldermann, I. Galan, F. Emmerich, F. Mittermayr, Effect of very high limestone content and quality on the sulfate resistance of blended cements, Constr. Build. Mater. 188 (2018) 1065–1076, https://doi.org/10.1016/j.conbuildmat.2018.08.169.

[4] T. Ikumi, S.H.P. Cavalaro, I. Segura, A. Aguado, Alternative methodology to consider damage and expansions in external sulfate attack modeling, Cem. Concr. Res. 63 (2014) 105–116, https://doi.org/10.1016/j.cemconres.2014.05.011.

[5] A. Neville, The confused world of sulfate attack on concrete, Cem. Concr. Res. 34 (2004) 1275–1296, https://doi.org/10.1016/j.cemconres.2004.04.004.

[6] M. Whittaker, L. Black, Current knowledge of external sulfate attack, Adv. Cem. Res. 27 (2015) 532–545, https://doi.org/10.1680/adcr.14.00089.

[7] T. Ikumi, S. Cavalaro, I. Segura, C. Goodier, S. Austin, Simplified analytical assessment of damaged induced by the external sulphate attack in concrete piles, in: High Tech Concr. Where Technol. Eng. Meet - Proc. 2017 Fib Symp., Springer International Publishing, Cham, 2017, pp. 2282–2289, https://doi.org/10.1007/978-3-319-59471-2_260.

[8] C. Yu, W. Sun, K. Scrivener, Mechanism of expansion of mortars immersed in sodium sulfate solutions, Cem. Concr. Res. 43 (2013) 105–111, https://doi.org/10.1016/j.cemconres.2012.10.001.

[9] P. Hagelia, R.G. Sibbick, N.J. Crammond, C.K. Larsen, Thaumasite and secondary calcite in some Norwegian concretes, Cem. Concr. Compos. 25 (2003) 1131–1140, https://doi.org/10.1016/S0958-9465(03)00143-4.

[10] P. Hagelia, R.G. Sibbick, Thaumasite sulfate attack, popcorn calcite deposition and acid attack in concrete stored at the «Blindtarmen» test site Oslo, from 1952 to 1982, Mater. Charact. 60 (2009) 686–699, https://doi.org/10.1016/j.matchar.2009.01.007.

[11] A.M. Ragab, M.A. Elgammal, O.A.G. Hodhod, T.E.S. Ahmed, Evaluation of field concrete deterioration under real conditions of seawater attack, Constr. Build. Mater. 119 (2016) 130–144, https://doi.org/10.1016/j.conbuildmat.2016.05.014.

[12] D. Wang, X. Zhou, Y. Meng, Z. Chen, Durability of concrete containing fly ash and silica fume against combined freezing-thawing and sulfate attack, Constr. Build. Mater. 147 (2017) 398–406, https://doi.org/10.1016/j.conbuildmat.2017.04.172.

[13] M. Collepardi, A state-of-the-art review on delayed ettringite attack on concrete, Cem. Concr. Compos. 25 (2003) 401–407, https://doi.org/10.1016/S0958-9465(02)00080-X.

[14] American Concrete Institute, ACI 201, 201.2R-08, Guide to Durable Concrete, 2008.

[15] Fédération internationale du béton. 2010. Fib model code for concrete structures 2010.

[16] Brazilian Association of Technical Standards, NBR 6118:2014. Design of concrete structures - Procedure, 2014.

[17] AENOR, UNE-EN 197-1:2011. Cement - Part 1: Composition, specifications and conformity criteria for common cements, 2011.

[18] T. Ikumi, I. Segura, S.H.P. Cavalaro, Effects of biaxial confinement in mortars exposed to external sulfate attack, Cem. Concr. Compos. 95 (2019) 111–127, https://doi.org/10.1016/j.cemconcomp.2018.10.017.

[19] I.G. Reyes, Characterization and control of wet-mix sprayed concrete with accelerators, 2013.

[20] C. Herrera, Evaluación de mezclas proyectadas: comportamiento y durabilidad, 2017.

[21] I. Galan, A. Baldermann, W. Kusterle, M. Dietzel, F. Mittermayr, Durability of shotcrete for underground support–Review and update, Constr. Build. Mater. 202 (2019) 465–493, https://doi.org/10.1016/j.conbuildmat.2018.12.151.

[22] R.P. Salvador, S.H.P. Cavalaro, R. Monte, A.D. Figueiredo, Relation between chemical processes and mechanical properties of sprayed cementitious matrices containing accelerators, Cem. Concr. Compos. 79 (2017) 117–132, https://doi.org/10.1016/j.cemconcomp.2017.02.002.

[23] R.P. Salvador, S.H.P. Cavalaro, M. Cano, A.D. Figueiredo, Influence of spraying on the early hydration of accelerated cement pastes, Cem. Concr. Res. 88 (2016) 7–19, https://doi.org/10.1016/j.cemconres.2016.06.005.

[24] R.P. Salvador, S.H.P. Cavalaro, I. Segura, G. Margarita, Relation between ultrasound measurements and phase evolution in accelerated cementitious matrices, Mater. Des. 113 (2017) 1–34, https://doi.org/10.1016/j.matdes.2016.10.022.

[25] C. Paglia, F. Wombacher, H. Böhni, M. Sommer, An evaluation of the sulfate resistance of cementitious material accelerated with alkali-free and alkaline admixtures: laboratory vs. field, Cem. Concr. Res. 32 (2002) 665–671, https://doi.org/10.1016/S0008-8846(01)00739-6.

[26] W. Kunther, B. Lothenbach, K.L. Scrivener, On the relevance of volume increase for the length changes of mortar bars in sulfate solutions, Cem. Concr. Res. 46 (2013) 23–29, https://doi.org/10.1016/j.cemconres.2013.01.002.

[27] T. Ikumi, S.H.P. Cavalaro, I. Segura, The role of porosity in external sulphate attack, Cem. Concr. Compos. 97 (2019) 1–12, https://doi.org/10.1016/j.cemconcomp.2018.12.016.

[28] H. Min, L. Sui, F. Xing, H. Tian, Y. Zhou, An effective transport model of sulfate attack in concrete, Constr. Build. Mater. 216 (2019) 365–378, https://doi.org/10.1016/j.conbuildmat.2019.04.218.

[29] R. Ragoug, O.O. Metalssi, F. Barberon, J.M. Torrenti, N. Roussel, L. Divet, J.B. d'Espinose de Lacaillerie, Durability of cement pastes exposed to external

sulfate attack and leaching: physical and chemical aspects, Cem. Concr. Res. 116 (2019) 134–145, https://doi.org/10.1016/j.cemconres.2018.11.006.
[30] W. Müllauer, R.E. Beddoe, D. Heinz, Sulfate attack expansion mechanisms, Cem. Concr. Res. 52 (2013) 208–215, https://doi.org/10.1016/j.cemconres.2013.07.005.
[31] A.M. Ramezanianpour, R.D. Hooton, Thaumasite sulfate attack in Portland and Portland-limestone cement mortars exposed to sulfate solution, Constr. Build. Mater. 40 (2013) 162–173, https://doi.org/10.1016/j.conbuildmat.2012.09.104.
[32] J. Haufe, A. Vollpracht, Tensile strength of concrete exposed to sulfate attack, Cem. Concr. Res. 116 (2019) 81–88, https://doi.org/10.1016/j.cemconres.2018.11.005.
[33] Z. Guo, Y. Wang, P. Hou, Y. Shao, X. Zuo, Q. Li, N. Xie, X. Cheng, Comparison study on the sulfate attack resistivity of cement-based materials modified with nanoSiO2 and conventional SCMs: mechanical strength and volume stability, Constr. Build. Mater. 211 (2019) 556–570, https://doi.org/10.1016/j.conbuildmat.2019.03.235.
[34] W. Kunther, B. Lothenbach, Improved volume stability of mortar bars exposed to magnesium sulfate in the presence of bicarbonate ions, Cem. Concr. Res. 109 (2018) 217–229, https://doi.org/10.1016/j.cemconres.2018.04.022.
[35] W. Kunther, B. Lothenbach, K. Scrivener, Influence of bicarbonate ions on the deterioration of mortar bars in sulfate solutions, Cem. Concr. Res. 44 (2013) 77–86, https://doi.org/10.1016/j.cemconres.2012.10.016.
[36] D.T. Niu, Y. De Wang, R. Ma, J. Bin Wang, S.H. Xu, Experiment study on the failure mechanism of dry-mix shotcrete under the combined actions of sulfate attack and drying-wetting cycles, Constr. Build. Mater. 81 (2015) 74–80, https://doi.org/10.1016/j.conbuildmat.2015.02.007.
[37] Z. Zhang, X. Jin, S. Lin, J. Bi, Direct shear behavior of sulfate-exposed shotcrete: experimental and modelling research, Constr. Build. Mater. 210 (2019) 607–619, https://doi.org/10.1016/j.conbuildmat.2019.03.229.
[38] W. Jiabin, N. Ditao, S. Zhanping, Damage layer thickness and formation mechanism of shotcrete with and without steel fiber under sulfate corrosion of dry–wet cycles by ultrasound plane testing method, Constr. Build. Mater. 123 (2016) 346–356, https://doi.org/10.1016/j.conbuildmat.2016.06.146.
[39] J. Wang, D. Niu, R. Ma, Y. Zhang, Investigation of sulfate attack resistance of shotcrete under dry-wet cycles, J. Wuhan Univ. Technol. Mater. Sci. Ed. 31 (2016) 1329–1335, https://doi.org/10.1007/s11595-016-1535-0.
[40] J. Wang, D. Niu, Y. Zhang, Mechanical properties, permeability and durability of accelerated shotcrete, Constr. Build. Mater. 95 (2015) 312–328, https://doi.org/10.1016/j.conbuildmat.2015.07.148.
[41] R.P. Salvador, D.A.S. Rambo, R.M. Bueno, K.T. Silva, A.D. de Figueiredo, On the use of blast-furnace slag in sprayed concrete applications, Constr. Build. Mater. 218 (2019) 543–555, https://doi.org/10.1016/j.conbuildmat.2019.05.132.
[42] AENOR, UNE-EN 196-2. Methods of Testing Cement. Part 2: Chemical Analysis of Cement, 2013.
[43] R.P. Salvador, S.H.P. Cavalaro, M.A. Cincotto, A.D. de Figueiredo, Parameters controlling early age hydration of cement pastes containing accelerators for sprayed concrete, Cem. Concr. Res. 89 (2016) 230–248, https://doi.org/10.1016/j.conbuildmat.2016.02.101.
[44] P.D. James Speight, Lange's Handbook of Chemistry, Sixteenth Edition, 16th ed., McGraw-Hill Education, New York, 2005. https://www.accessengineeringlibrary.com/content/book/9780071432207.
[45] UNE-EN, EN 206-1. Concrete – Part 1: Specification, performance, production and conformity, 2013.
[46] T. Ikumi, I. Segura, Numerical assessment of external sulfate attack in concrete structures. A review, Cem. Concr. Res. 121 (2019) 91–105, https://doi.org/10.1016/j.cemconres.2019.04.010.
[47] F. Bellmann, B. Möser, J. Stark, Influence of sulfate solution concentration on the formation of gypsum in sulfate resistance test specimen, Cem. Concr. Res. 36 (2006) 358–363, https://doi.org/10.1016/j.cemconres.2005.04.006.
[48] R. El-Hachem, E. Rozire, F. Grondin, A. Loukili, New procedure to investigate external sulphate attack on cementitious materials, Cem. Concr. Compos. 34 (2012) 357–364, https://doi.org/10.1016/j.cemconcomp.2011.11.010.
[49] T. Ikumi, New insights on the fundamentals and modeling of the external sulfate attack in concrete structures, 2017.
[50] R. Snellings, X-ray powder diffraction applied to cement, in: A Pract. Guid. to Microstruct. Anal. Cem. Mater., CRC Press, 2015: pp. 107–176. doi:10.1201/b19074-5.
[51] B. Lothenbach, P. Durdzinski, K.D.E. Weerdt, Thermogravimetric analysis, in: A Pract. Guid. to Microstruct. Anal. Cem. Mater., CRC Press, 2015: pp. 177–212. doi:10.1201/b19074-6.
[52] K. Scrivener, A. Bazzoni, B. Mota, J. Rossen, Electron microscopy, in: A Pract. Guid. to Microstruct. Anal. Cem. Mater., CRC Press, 2015: pp. 351–418. doi:10.1201/b19074-9.
[53] ASTM, ASTM: C490 Standard Practice for Use of Apparatus for the Determination of Length Change of Hardened Cement Paste , Mortar , and Concrete 1, ASTM Int. (2008) 1–5.
[54] AENOR, UNE 83980. Concrete durability. Test methods. Determination of the water absorption, density and accessible porosity for water in concrete, (2014) 6.
[55] AENOR, UNE-EN 12390-3. Testing hardened concrete. Part 3: Compressive strength of test specimens, (2009) 20.
[56] M.H. Maciel, G.S. Soares, R.C. de O. Romano, M.A. Cincotto, Monitoring of Portland cement chemical reaction and quantification of the hydrated products by XRD and TG in function of the stoppage hydration technique, J. Therm. Anal. Calorim. (2018), https://doi.org/10.1007/s10973-018-7734-5.
[57] T. Schmidt, B. Lothenbach, M. Romer, J. Neuenschwander, K. Scrivener, Physical and microstructural aspects of sulfate attack on ordinary and limestone blended Portland cements, Cem. Concr. Res. 39 (2009) 1111–1121, https://doi.org/10.1016/j.cemconres.2009.08.005.
[58] R.J. Flatt, G.W. Scherer, Thermodynamics of crystallization stresses in DEF, Cem. Concr. Res. 38 (2008) 325–336, https://doi.org/10.1016/j.cemconres.2007.10.002.
[59] G.W. Scherer, Stress from crystallization of salt, Cem. Concr. Res. 34 (2004) 1613–1624, https://doi.org/10.1016/j.cemconres.2003.12.034.
[60] C. Herrera-Mesen, R.P. Salvador, S.H.P. Cavalaro, A. Aguado, Effect of gypsum content in sprayed cementitious matrices: early age hydration and mechanical properties, Cem. Concr. Compos. 95 (2019) 81–91, https://doi.org/10.1016/j.cemconcomp.2018.10.015.
[61] C. Lian, Y. Zhuge, S. Beecham, The relationship between porosity and strength for porous concrete, Constr. Build. Mater. 25 (2011) 4294–4298, https://doi.org/10.1016/j.conbuildmat.2011.05.005.